Nonlinear Dependence of the Contact Angle of Nanodroplets on Contact Line Curvature

Antonio Checco and Patrick Guenoun
Service de Physique de l'Etat Condensé, C.E.A. Saclay, F-91191 Gif-sur-Yvette CEDEX, France

Jean Daillant
Service de Physique de l'Etat Condensé, C.E.A. Saclay, F-91191 Gif-sur-Yvette CEDEX, France
and LURE, CNRS/CEA/MJENR, Bâtiment 209D, Centre Universitaire Paris-Sud, F-91898 Orsay CEDEX, France
(Received 22 May 2003; published 31 October 2003)

We have measured the contact angle of microsized and nanosized alkane droplets partially wetting a model substrate using true noncontact atomic force microscopy. The large range of droplet sizes accessible using this technique allowed us to determine the contact line curvature dependence of the contact angle with unprecedented accuracy. Whereas previous studies aimed at explaining such a dependence by a line tension effect, our results and calculations on a model system exclude such an effect and point to an extreme sensitivity to weak substrate heterogeneities confirmed by numerical simulations.

DOI: 10.1103/PhysRevLett.91.186101 PACS numbers: 68.08.Bc, 68.37.Ps

Whereas wetting phenomena are well understood at the macroscopic scale, fascinating new phenomena might occur when nanometric spatial dimensions come into play. For example, a negative line energy, a concept introduced by Gibbs more than one century ago [1] but still controversial after a century of theoretical and experimental effort [2], could make a surface more and more wettable when smaller droplets are considered. Beyond their fundamental interest, such questions are also technologically relevant, for example, in soft lithography techniques [3,4] or for micro- and nanofluidics applications such as labs on chips [5]. Even on simple homogeneous substrates, however, wetting mechanisms have not received a full understanding and description when such small spatial scales come into play.

The size-dependent apparent contact angle at small scales is described using a "modified Young equation" [6]:

$$\cos\theta = \frac{\gamma_{SV} - \gamma_{SL}}{\gamma_{LV}} - \frac{\tau}{\gamma_{LV} r} = \cos\theta_\infty - \frac{\tau}{\gamma_{LV} r}. \quad (1)$$

Equation (1) relates the variation of the apparent contact angle θ to the contact line radius r. τ is known as the line tension, γ_{SV} is the solid-vapor surface energy, γ_{SL} the solid-liquid surface energy, and γ_{LV} the surface tension. Equation (1) shows that wetting phenomena can strongly depend on scale.

Line tension is usually calculated as the free energy correction due to the modification of the droplet profile close to the contact line by van der Waals forces (interface displacement model [7–9]), and is expected to be on the order of τ/γ_{LV}. On the other hand, the positive or negative experimental values measured in the context of the size dependence of the contact angle of microscopic droplets, nucleation on solid surfaces, Newton black films, and foams span over 7 orders of magnitude from 10^{-12} to 10^{-5} N [2]. The smallest values on the order of 10^{-12} N, closest to the theoretical estimations (see below), are obtained when only liquid phases are involved, as in the case of soap films. The largest values are, on the contrary, obtained for liquid droplets on solid substrates, suggesting that van der Waals forces cannot be the only origin of the size dependence of contact angles on solid surfaces. In particular, surface heterogeneity was proposed to be an important parameter [10–14]. In this context, local profilometry by atomic force microscopy (AFM) has been used in order to investigate smaller length scales. An elaborate method taking advantage of a striped wettability pattern to get high contact line curvatures was used in Ref. [15]. The line tension values found in this study $\approx 10^{-10}$ N were much smaller than generally found but still larger than theoretically expected, while deviations of the droplet profile from a spherical cap close to the contact line extend far larger than the expected range τ/γ_{LV}.

Previous AFM experiments used the intermittent contact mode and were not devoted to the study of model wetting systems involving simple solid-liquid interactions. This has prevented any direct comparison to theory and therefore any identification of the origin of the curvature dependence of contact angle. To address these points, we chose to study widely used model substrates, namely, silanized silicon wafers and low molecular weight ($9 \leq n \leq 12$) n-alkane droplets, therefore ensuring minimal heterogeneity and pure van der Waals interactions. Silanized substrates were first prepared by distillation of octadecyltrichlorosilane and coating silicon wafers according to standard methods [16]. Deposition temperature was 8° and the critical surface tension was 20.07 mN/m. In such a way, flat, smooth (rms roughness about 1 Å over 5×5 μm as measured by tapping mode AFM), chemically homogeneous, low

energy surfaces exhibiting low hysteresis (1°–2°) were obtained. Because of the volatility of alkanes, stable droplets cannot be formed under ambient conditions. We therefore designed an evaporation-condensation chamber connected to the AFM scanning head and containing the substrate. This enables an optimal use of AFM capabilities by investigating the largest possible range of equilibrium droplet sizes [Figs. 1(a)–1(c)]. The droplet topographies were obtained using noncontact [17] atomic force microscopy (NC-AFM). We used a TM Microscopes M5 AFM using a 100 μm scanner equipped with commercial Ultrasharp TM ($110 \times 35 \times 2$) μm^3 rectangular silicon cantilevers with a long ~ 10 μm tip in order to minimize acoustic effects [18]. Their nominal spring constant was 7.5 N/m while the resonance frequency and the quality factor were measured to be 271 kHz and 250, respectively. The imaging technique consists in exciting the cantilever slightly above its resonance frequency. The sample force field induces a reduction in the oscillation amplitude compared to the free amplitude A_{free} [17]. Sample topography is reconstructed by maintaining constant a given setpoint amplitude A_{sp} while scanning the sample. Strict experimental conditions must be set to get a stable drop profile: $A_{\text{free}} < 10$ nm to avoid any tip capture, and $A_{sp} \approx 0.9 \times A_{\text{free}}$ for sensitivity. We also recorded the phase of the cantilever oscillation relative to the drive [Fig. 2(b)]. The phase contrast on the drops is small (a few degrees), and is correlated to transient effects of the feedback loop [Fig. 2(c)] [19]. In any case, the observed range of phase variations ensures that the energy dissipated by the tip-liquid interaction is negligible [20] as expected for NC-AFM. This small interaction is not obtained at the expense of lateral resolution as in methods making use of longer range interactions [21].

Our droplet profiles can be nicely fitted to a spherical cap [Fig. 2(a)] providing an accurate determination of the contact angle and contact line radius. The experimental errors mainly come from nonlinearities of the piezoelectric scanner, which are minimized by an optical control of the actual scanner displacement, and from tip-sample convolution effects. The convolution results in an overall dilation of the profile and a smoothening near the contact line. Using a numerical deconvolution technique [22], we estimate that, for our tips with 30 to 50 nm curvature radii determined by scanning electron microscopy, the error is 10 nm on droplet radii and goes from 0.1° for

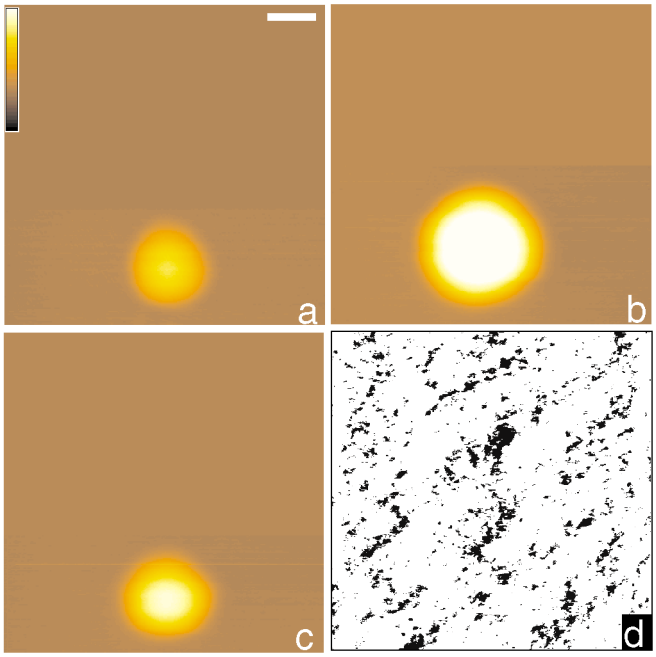

FIG. 1 (color online). Volume control of a submicron decane droplet; in (a) decane vapor has been injected into the chamber and the drop inflates to (b); in (b) reducing the pressure droplet evaporates to (c). The images are 256×256 pixels and were acquired using a scanning frequency of 0.5 line per second. (d) Digitized surface for the simulation described in the text. The horizontal bar is 1 μm and the vertical bar is 20 nm.

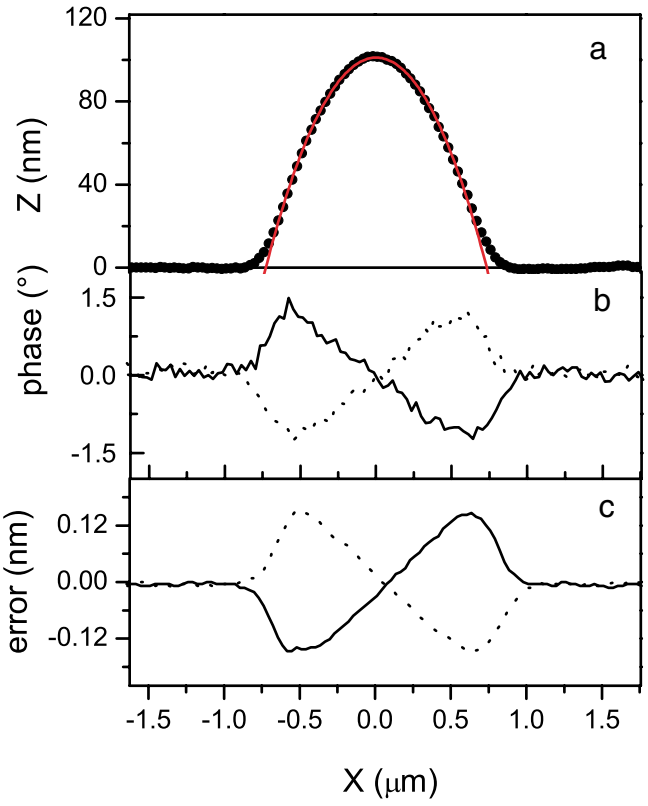

FIG. 2 (color online). (a) Experimental profile of a droplet (points) and fit to a spherical cap (line). (b) Phase of the cantilever oscillation relative to the drive. (c) Error signal (difference between the actual amplitude of the oscillation and the work amplitude). This error signal is maximum when the slope is maximum. In (b) and (c), continuous lines are for scanning from left to right and dotted lines from right to left.

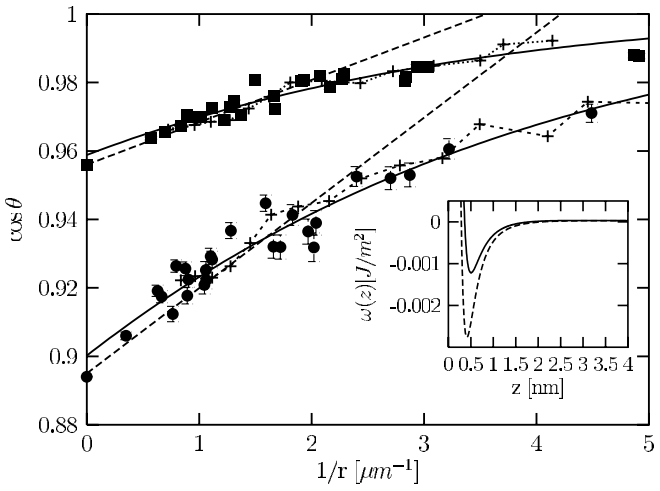

FIG. 3. Cosine of the contact angle versus the inverse of the contact line radius for nonane (squares) and dodecane (circles) droplets on a silanized wafer. The +-and-dotted line is the result of a simulation as described in the text. The dashed lines are a fit to Eq. (1) and the continuous lines are a fit to $\cos\theta = 1 + (S/\gamma)(1 - \delta r/r)^6$. Inset: Effective potential for nonane (line) and dodecane (dashed line).

largest drops to 0.4° for smallest ones on the contact angle.

The cosine of the contact angle is plotted versus the inverse of the contact line radius in Fig. 3. For all alkanes, the contact angle decreases with decreasing drop radius from its macroscopic value determined by fitting digital photographs of millimeter sized drops under alkane saturated atmosphere. We did not observe any increase in contact angle hysteresis at the small length scales investigated here. Using NC-AFM, the profiles of droplets much smaller (down to 150 nm) than in previous studies [9] could be recorded, allowing a precise comparison with Eq. (1). An important result of this paper is that the modified Young equation which would lead to a straight line in Fig. 3 does not correctly describe the experimental data when a large enough range of droplet sizes is considered.

As a first step in the analysis, we have calculated the intrinsic line tension due to van der Waals forces for our system using an effective interface potential $\omega(l)$ [23] modified to take the silane film into account (Fig. 3 inset). $\omega(l) = -32/9\epsilon\rho^2\sigma^4[1 + (l - d_w)/\sigma\{\arctan[(l - d_w)/\sigma] - \pi/2\} - \sigma^2/3l^2] + (A_{al\text{-Si}} - A_{al\text{-SiO}_2})/(l + d_{sil} + d_{\text{SiO}_2})^2 + (A_{al\text{-SiO}_2} - A_{al\text{-}sil})/(l + d_{sil})^2 + (A_{al\text{-}sil} - A_{al\text{-}al})/l^2$. The first term describes the confined liquid interactions in a film of thickness l beyond the l^{-2} term; taking the example of dodecane, one has $\epsilon = 2.9 \times 10^{-22}$ J calculated from the dodecane-dodecane Hamaker constant, ρ is the dodecane density, $\sigma \approx 0.41$ nm is the dodecane core radius chosen in order to get the correct value of the minimum of the potential ($S = -2.75$ mN/m), and $d_w \approx 0.2$ nm is the minimum substrate-decane distance. The second term describes the substrate-alkane interactions with the silica and silane thicknesses $d_{\text{SiO}_2} = 2$ nm, $d_{sil} = 2.3$ nm and $A_{al\text{-Si}} - A_{al\text{-SiO}_2} = 0.44 \times 10^{-21}$ J, $A_{al\text{-SiO}_2} - A_{al\text{-}sil} = 2.5 \times 10^{-21}$ J, $A_{al\text{-}sil} - A_{al\text{-}al} = 0.13 \times 10^{-21}$ J. These values were obtained using Hamaker constants for silicon, silica, silane, and alkanes: $A_{\text{Si}} = 23 \times 10^{-20}$ J [24], $A_{\text{SiO}_2} = 20 \times 10^{-20}$ J [24], $A_{sil} = 7 \times 10^{-20}$ J [25], $A_{al} = 6.7 \times 10^{-20}$ J [25], for dodecane and standard combination rules [24].

The line tension has then been calculated in two ways. First, we used the method of Ref. [23] which carefully identifies the contributions to the line energy. Using this method, we obtain $\tau = -2.3 \times 10^{-12}$ N for dodecane, whereas an (unsatisfactory) linear fit to the data would yield much larger values (-5×10^{-10} N). We have also checked that the interface displacement model [7–9], valid in the limit of small contact angles, yields a consistent estimate of line tension in that case: $\tau = -2.0 \times 10^{-12}$ N. This is very important since this method which consists in estimating the increase in surface energy and potential energy at the contact line amounts after minimization to integrating the square root of the effective potential $\omega(l)$ from its minimum in l_0 to infinity, $\tau = \sqrt{2\gamma_{\text{LV}}} \int_{l_0}^{\infty} dl[\sqrt{\omega(l) - S} - \sqrt{-S}]$. The line tension value is therefore strongly constrained by the value of the potential at the origin $\omega(l_0) = S = \gamma_{SV} - \gamma_{SL} - \gamma_{\text{LV}}$, and the range of its decay to 0 which must be a few nm for van der Waals forces. This proves that the line tension cannot be larger than a few 10^{-12} N. We finally checked that the effect of contact line curvature [26] is negligible. All this shows that our results, and more generally all measurements on solid substrates, can in no way be explained as being an intrinsic line tension effect.

We propose below an alternative description based on substrate heterogeneity according to the following scenario: Droplets are nucleated on the highest energy defects, then grow preferentially on the most wettable areas, possibly slightly shifting their center of mass, in order to minimize the free energy. This tendency is balanced by surface tension which acts as an elastic restoring force [11] maintaining an approximately spherical shape as observed in Figs. 2(a)–2(c). This is a case of weak heterogeneities, as discussed by Joanny and de Gennes [10], where nearly no hysteresis is induced and fluctuations of the contact line are small at the observation scale. Our method is fundamentally different from Cassie's method [27] since individual droplets which minimize their free energy on the actual surface are considered instead of average values. In order to be more quantitative, we have calculated the equilibrium radius of spherical droplets randomly placed on the heterogeneous substrate. For simplicity, we have considered a binarized AFM image of our substrate [Fig. 1(d)] with two different values of the spreading parameter for dodecane $S_1 = -2.75$ mN/m [corresponding to the white region in Fig. 1(d) with

surface coverage 0.9] and slightly wetting patches with $S_2 = 0.5$ mN/m (surface coverage 0.1) corresponding to mixed exposed groups of CH_2 and CH_3 (the critical surface energy of self-assembled silane monolayers is 20.5 mN/m [28], whereas that of a polyethylene surface partially exposing its CH_2 groups is 31 mN/m [29] and dodecane surface tension is 25.3 mN/m). Neglecting long-range forces, the free energy of a spherical cap on the heterogeneous substrate is $F = \pi r^2 \gamma (1 - \cos\theta)^2 / \sin^2\theta - \pi r^2 [cS_1 + (1 - c)S_2]$. Minimizing this free energy, we can estimate the equilibrium size of a spherical droplet of a given volume centered at a fixed point on the heterogeneous substrate. We proceed by calculating the free energy of 2000 fixed volume droplets randomly placed on the substrate and, for each of them, we determine r and θ giving the lowest free energy. In order to retain only the most favorable nucleation sites, we then calculate the contact angle corresponding to this droplet volume as the average over the 50 sites leading to the lowest free energy values (Fig. 3). Of course, this calculation is crude; we consider only spherical droplets (which is justified experimentally) and the pixel size may introduce a distortion for the smallest droplets. However, this calculation gives a correct description of our data, thus supporting our interpretation. In particular, the range of contact angle variation from the macroscopic value to smaller values for smaller droplets is good. Similar calculations on simulated surfaces show that the contact angle variation sensibly depends on surface correlations which gives confidence that this model captures the essential features of the problem.

Droplet deformation can be more thoroughly investigated by comparing the experimental droplet radius r to the radius r_0 of a droplet having the same volume $V = 1/3\pi r_0^3 (2 - 3\cos\theta_\infty + \cos^3\theta_\infty)/(1 - \cos^2\theta_\infty)^{3/2}$ and the macroscopic contact angle θ_∞ [Eq. (1)]. Surprisingly, $\delta r = r - r_0$ is found constant for a given alkane; we find $\delta r \approx 48$ nm for nonane, $\delta r \approx 47$ nm for decane, $\delta r \approx 41$ nm for dodecane. To first order, this implies $\cos\theta = 1 + (S/\gamma)(1 - \delta r/r)^6$, which describes well the experimental data (Fig. 3). Such values of $\delta r \approx 40$–50 nm again point out to substrate heterogeneities, since it is not possible to construct such a length from perfect substrate-liquid interactions (for $\tau \approx 10^{-11}$ N and $\gamma_{LV} \approx 20$ mN/m, one would expect $\delta r \approx \tau/\gamma \approx 0.5$ nm, in agreement with our model calculations). We also note that δr decreases from nonane to dodecane, a consistent result if the restoring force is the surface tension.

It was demonstrated in this paper that NC-AFM can quantitatively investigate the dynamics and statics of wetting *of true liquids* at small scales without perturbation. Wetting of nanopatterned substrates, essential for applications in microfluidics, for instance, rather necessitates a control and a knowledge of the defects distribution, even for low hysteretic substrates. Numerical approaches such as the one developed here should appear essential in future developments.

We thank J. Creuze, LURE, for providing us numerical surfaces to test our model.

[1] J. Gibbs, *The Scientific Papers* (Dover, New-York, 1961), Vol. 1.
[2] J. Drelich, Colloids Surf. A **116**, 43 (1996).
[3] R. Peters, X. Yang, T. Kim, B. Sohn, and P. Nealey, Langmuir **16**, 4625 (2000).
[4] W. Lopes and H. Jaeger, Nature (London) **414**, 735 (2001).
[5] G. Whitesides and A. Stroock, Phys. Today **54**, 42 (2001).
[6] L. Boruvka and A. Neumann, J. Chem. Phys. **66**, 5464 (1977).
[7] P. de Gennes, Rev. Mod. Phys. **57**, 827 (1985).
[8] H. Dobbs and J. Indekeu, Physica (Amsterdam) **201A**, 457 (1993).
[9] J. Wang, S. Betelu, and B. Law, Phys. Rev. E **63**, 031601 (2001).
[10] J. Joanny and P. de Gennes, J. Chem. Phys. **81**, 552 (1984).
[11] M. Robbins and J. Joanny, Europhys. Lett. **3**, 729 (1987).
[12] D. Li, F. Lin, and A. Neumann, J. Colloid Interface Sci. **142**, 224 (1991).
[13] A. Marmur, Colloids Surf. A **136**, 81 (1998).
[14] G. Wolansky and A. Marmur, Langmuir **14**, 5292 (1998).
[15] T. Pompe and S. Herminghaus, Phys. Rev. Lett. **85**, 1930 (2000).
[16] J. Brzoska, N. Shahidzadeh, and F. Rondelez, Nature (London) **360**, 719 (1992).
[17] Y. Martin, C. Williams, and H. Wickramasinghe, J. Appl. Phys. **61**, 4723 (1987).
[18] P. Fontaine, P. Guenoun, and J. Daillant, Rev. Sci. Instrum. **68**, 4145 (1997).
[19] O. Marti, in *Procedures in Scanning Probe Microscopy*, edited by R. Colton, A. Engel, and J. Frommer (Wiley, New-York, 1998), p. 109.
[20] J. Cleveland, B. Anczykowski, A. Schmid, and V. Elings, Appl. Phys. Lett. **72**, 2613 (1998).
[21] F. Rieutord and M. Salmeron, J. Phys. Chem. B **37**, 3941 (1998).
[22] D. Keller, Surf. Sci. **294**, 409 (1993).
[23] T. Getta and S. Dietrich, Phys. Rev. E **57**, 655 (1998).
[24] J. Visser, Adv. Colloid Interface Sci. **3**, 331 (1972).
[25] T. Ederth, Langmuir **17**, 3329 (2001).
[26] H. Dobbs, Int. J. Mod. Phys. B **13**, 3255 (1999).
[27] A. Cassie, Discuss. Faraday Soc. **57**, 5041 (1952).
[28] J. Brzoska, I. Ben Azouz, and F. Rondelez, Langmuir **10**, 4367 (1994).
[29] W. Zisman, in *Contact Angle, Wettability and Adhesion*, edited by F. Fowkes, Advances in Chemistry Series Vol. 43 (American Chemical Society, Washington, DC, 1964), p. 21.